Earthquake Geotechnical Engineering for Protection and Development of Environment and Constructions – Silvestri & Moraci (Eds)
© 2019 Associazione Geotecnica Italiana, Rome, Italy, ISBN 978-0-367-14328-2

Assessing seismically induced slope deformation of the Diezma landslide via limit equilibrium analysis and numerical modeling

G. Domej
IFSTTAR – GERS – Laboratoire Séismes et Vibrations, Champs-sur-Marne, France

C. Bourdeau
IFSTTAR – GERS – Laboratoire Sol, Roches et Ouvrages Géotechniques, Champs-sur-Marne, France

L. Lenti
IFSTTAR – GERS – Laboratoire Séismes et Vibrations, Champs-sur-Marne, France

S. Martino
Università di Roma Sapienza, Dipartimento di Scienze della Terra & CERI, Rome, Italy

J. Delgado Marchal
Universidad de Alicante, Departamento Ciencias de la Tierra y del Medio Ambiente, Alicante, Spain

ABSTRACT: Earthquake-triggered slope deformation constitutes a major threat in seismic regions. It is therefore of major interest to properly evaluate expected displacements to ensure appropriate surveillance of concerned slopes. In order to assess and compare deformation patterns along slope surfaces, a series of different seismic scenarios was applied to the case study site of the Diezma Landslide using three different methods: the Newmark-Method (1965) being the only type of analysis based on the limit-equilibrium principle; simple estimation by modal recombination in the frequency domain with the finite element code CESAR-LCPC 2D under visco-elastic conditions; and analysis in the time domain with the finite difference code FLAC 2D under elasto-plastic conditions. This work discusses results obtained by the three mentioned methods and permits a critical view on the suitability and the scenario-sensitivity of each of the three methods.

1 INTRODUCTION

With the aim of contributing to a better understanding of standard procedures for dynamic analysis of slopes undergoing seismic shaking, this study presents the application of one analogue and two numerical methods to the Diezma Landslide, which represents a classic case of a translational landslide according to the classification of Varnes (1978). The impact of eleven seismic scenarios on the slope is modeled, on the one hand, using the worldwide common reference method – the Newmark-Method (1965) – and compared, on the other hand, to the performance of two linear-numerical approaches: analysis with the modal recombination method (MRM) and stress-strain-analysis with the finite difference method (FDM).

This work presents in a first stage the choice of the Diezma Landslide as suitable case study. Furthermore, the applied signals are characterized and a short theoretical background is given for each of the three methods before discussing the performance of the methods as well as the respective estimated internal and superficial deformation patterns.

2 LANDSLIDE SITE, SIGNALS AND APPLIED METHODS

2.1 *The Diezma landslide*

Located 25 km northeast of Granada (Figure 1; 37°18′37.0″N, 3°22‘10.5"W), Southern Spain, the medium sized translational Diezma Landslide with its 1.2 million m³ is adjacent to the A-92 motorway. Being active since the 1990s, it experienced its main failure on 18th of March 2001 after the completion of the motorway road cut and a heavy rain period.

So far, there are no reports of seismically induced deformation for the site. However, due to its location in a zone of major seismicity (Martínez-Solares et al. 2013), authors consider a seismic impact on the landslide very likely (Martino et al. 2016) what makes the landslide a suitable case study.

Consisting of Cretaceous to Lower Miocene flysch with clays, silts, marls and embedded blocks, the landslide mass is exceptionally well documented in geologic terms (Table 1) as well as by geotechnical and geophysical prospection of several authors (Azañon et al. 2010, Rodríguez-Peces et al. 2011, Delgado et al. 2015, Martino et al. 2016).

A detailed engineering-geological model of the landslide mass is given by diverse cross sections (Delgado et al. 2015), of which the longitudinal cross section in the main sliding

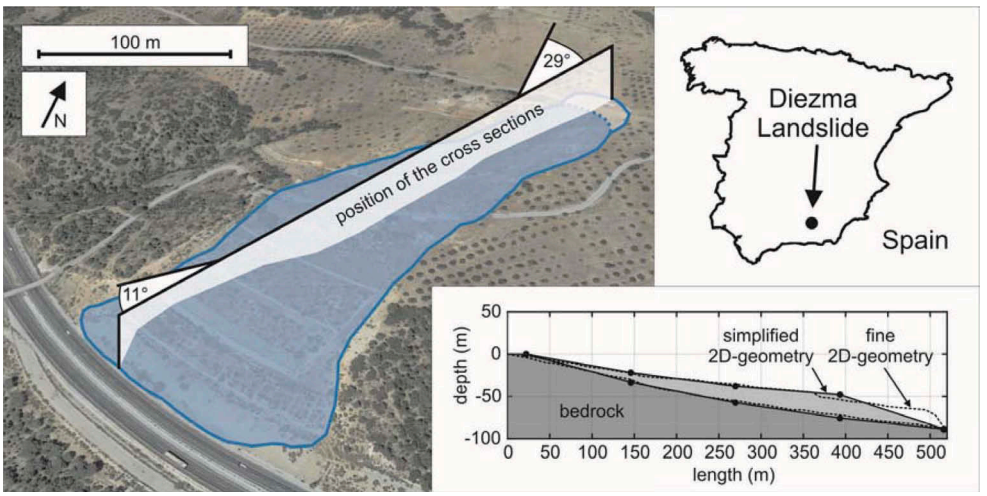

Figure 1. Location of the Diezma Landslide and its cross sections; the offset from north is 29° eastwards and the mean slope angle is 11° (after Google Earth 2015). In the simplified cross section, the thick dots indicate the sectioning proposed by Domej et al. (2017) to outline rupture zones of landslides.

Table 1. Geotechnical properties (after Delgado et al. 2015 & Rodríguez-Peces et al. 2011).

	Dry specific weight γ	Saturated specific weight $\gamma_{saturated}$	Peak cohesion c_{peak}	Residual cohesion $c_{residual}$	Peak friction angle Φ_{peak}	Residual friction angle $\Phi_{residual}$	Shear wave velocity v_s	Poisson's Ratio ν
Geotechnical unit	kN/m³	kN/m³	kPa	kPa	°	°	m/s	(-)
landslide	19.0	21.4*	46.0	4.0*	26.0	12.0*	300	0.25
sliding surface	15.2	17.7	01.3	0.4	21.0	08.0	300	0.25
bedrock	18.2	20.6	05.4	0.6	31.0	11.0	750**	0.35

* calibrated by Delgado et al. (2015)/
** set to 1000 m/s in FLAC for better impedance contrast

direction was adapted into a simplified and a fine version (upper subplots in Figure 1). Both cross sections correspond to the state of the slope after the road cut and before the main failure; the simplified version was outlined according to the four-slice-sectioning proposed by Domej et al. (2017) that approximates rupture zones of landslides (thick dots in Figure 3a).

2.2 *Signals*

For the assessment of seismically induced slope deformation a series of eleven signals (Table 2) was filtered from the European Strong-Motion Database (ESMD; Ambraseys et al. 2004) by application of the following criteria that reflect the local seismicity in Southern Spain with respect to a return period of 475 years:

- Arias Intensities (AI): 0.1 – 0.3 m/s (adapted from Delgado et al. 2015)
- peak ground accelerations (PGA): 0.6 - 1.2 m/s² (adapted from Benito et al. 2010)
- only horizontal components

The last criterion is simply owed to uniformity and component availability of three-component strong-motion records. Here the assumption is, that the imaginary hypocenter is sufficiently far away from the Diezma Landslide to ensure vertical incidence of the signal towards the ground surface. The reason for the use of the ESMD is the fact that there are no records of strong earthquakes ($M_W > 5$) during the last decades in the area of the landslide (Martino et al. 2016).

All signals have undergone a 4^{th}-order low-pass Butterworth-Filter with a cut-off-frequency of 10 Hz to obtain representative Fourier Amplitude Spectra (FAS) in terms of frequency content on the one hand, and to allow for suitable signal propagation by the two numerical methods.

2.3 *Applied methods*

The Newmark-Method (1965) uses the analogy between a potential landslide mass sliding on a pre-defined plane of weakness (sliding surface for Diezma landslide, see Table 1) and a rigid block resting on an inclined plane to develop a methodology for predicting the permanent displacement of a slope subjected to any ground motion. It makes use of the pseudo-static limit equilibrium method to derive the pseudo-static safety factor SF representing the dynamic aspect of the earthquake as an additional horizontal body force. Considering that the dimensions of the Diezma landslide (planimetric length more than ten times its maximal depth) make it a suitable candidate for the application of the "infinite slope scheme", we calculated the pseudo-static coefficient SF weighing the sum of all holding against the sum of all driving forces applying to the gravity center of the block:

Table 2. Series of eleven signals filtered form the ESMD (Ambraseys et al. 2004).

	ESMD			M_W	PGA	PGV	PGD	AI
Signal	number*	Earthquake	Date	(-)	m/s²	m/s	m	m/s
A	000049x	Friuli	1976-05-06	6.53	0.61	0.08	0.02	0.12
B	000133x	Friuli**	1976-09-15	6.04	1.07	0.10	0.02	0.12
C	000127x	Friuli**	1976-09-15	6.04	1.03	0.05	0.00	0.14
D	000294x	Campano Lucano	1980-11-23	6.93	0.91	0.18	0.06	0.27
E	000335x	Alkion	1981-02-25	6.38	1.14	0.11	0.03	0.22
F	001875x	Griva	1990-12-21	6.15	0.98	0.11	0.01	0.13
G	006142x	Aigion	1995-06-15	6.52	0.80	0.14	0.04	0.19
H	000599x	Umbria Marche	1997-09-26	5.72	0.96	0.05	0.01	0.13
I	000612x	Umbria Marche	1997-09-26	6.04	0.93	0.14	0.05	0.23
J	000625x	Umbria Marche**	1997-10-06	5.58	1.05	0.07	0.01	0.12
K	005820x	Strofades	1997-11-18	6.64	0.70	0.07	0.02	0.13

* x-components of the seismic records/
** aftershocks

$$SF = \frac{c \cdot \frac{dx}{\cos(\beta)} + (N - k_h \cdot W \cdot \sin(\beta)) \cdot \tan(\Phi)}{W \cdot \sin(\beta) + k_h \cdot W \cdot \cos(\beta)} = \frac{holding\ forces}{driving\ forces} \quad (1)$$

where W = weight of the block (N); N = normal force onto the plane (N);
c = cohesion (Pa); dx = projected length of the block to the horizontal (m);
β = slope angle (°); Φ = internal friction angle (°); k_h = pseudo-static coefficient (-)

Assuming that motion occurs only when SF ≤ 1, the critical k_h-value (k_c) can be deducted (for SF = 1). It is multiplied by the gravity constant (9.81 m/s²) to obtain the critical acceleration (a_c = k_c * g) that the block must overcome in order to move downslope. This information together with an accelerometric record is then processed – e.g. – with the software SLAMMER (Jibson et al. 2013); via double integration one value of cumulative downslope displacement is calculated for the entire block that represents the final state when the block has come to rest again.

Using the concept of numerical finite element methods (FEM), the MRM operates in the frequency domain and is originally designed for structural dynamics (Pecker, 2018). It calculates the response of an oscillator (i.e. the landslide) of n degrees of freedom (DOF) to an external load (i.e. an earthquake) with respect to the foundation (i.e. the bedrock). Being an implicit formulation, the method assumes visco-elastic material behavior represented by the matrix-based equation of a forced and damped vibratory motion:

$$\underbrace{\underline{M} \cdot \left(\ddot{\underline{U}} + \ddot{\underline{Y}}\right)}_{\text{internal force}} + \underbrace{\underline{C} \cdot \dot{\underline{U}}}_{\text{viscousforce}} + \underbrace{\underline{K} \cdot \underline{U}}_{\text{elasticforce}} = \underline{0} \quad (2)$$

where $\underline{M}$ = mass matrix (kg); $\underline{C}$ = damping matrix (kg/s); $\underline{K}$ = stiffness matrix (N/m);
$\underline{U}$ = displacement vector (relative to the foundation; m);
$\underline{Y}$ = displacement vector (caused by the earthquake; m)

The principle of the method is to conduct the computation of the total displacement based on a combination of eigenmodes. The latter are calculated with the software CESAR-LCPC 2D (iTech & IFSTTAR 2014) – as first stage – in a modal analysis of the structure revealing its eigenfrequencies; in a second stage, the response of the structure to an external load is evaluated giving one value of maximum displacement per mesh point.

The numerical FDM operates in the time domain. As a common tool in geotechnical engineering, it discretizes the structure of interest (i.e. the landslide) into a finite number of zones to which stresses and strains are applied via finite difference equations; these equations are then solved for displacement assuming visco-elasto-perfectly-plastic material behavior. Being an explicit formulation, computations are executed in short time increment cycles by the software FLAC 2D (ITASCA 2012). The procedure is carried out in two steps: the preceding static evaluation of the slope calculates the settlement due to gravity, whereas the second dynamic evaluation assesses the response of the structure to seismic shaking. Results appear in the form of one value of residual displacement per mesh point.

3 DISCUSSION OF RESULTS PER METHOD

3.1 *Newmark-method (1965)*

In terms of model layout, the Newmark-Method (1965) is much simpler than its numerical counterparts. Accounting only for block dimensions, slope angle, weight, cohesion and internal friction angle (calibrated values in Table 1) the method misses out macro-seismic parameters as well as the shear wave velocity of the landslide mass. It represents neither the lateral confinement nor the internal deformation during downslope motion. Another critical issue is the dependency of the estimated displacements on the critical acceleration which effectively limits the influence of frequency content and duration of the applied signals.

For each signal and based on a critical acceleration (a_c) of 0.6 m/s², displacements were evaluated for the normal and the inverse polarity, of which the respective maximum was

retained (first column of Table 3). Throughout the eleven signals, estimated displacements range from 0.0 to 1.4 cm.

3.2 *Modal Recombination Method (MRM)*

Accounting for material properties (Table 1) such as shear wave velocity, Poisson's Ratio, shear modulus and Young's Modulus, the numerical code CESAR-LCPC 2D is clearly incorporating more relevant information about the landslide mass. Yet nonlinear behavior of soils is not accounted for in MRM; therefore co-seismic displacements calculated with this method may over-estimate the amplitude of ground-motions in particular when very large strains develop in the landslide. The model layout consists of a triangular grid for the simplified geometry with a spacing of 0.5 m and rigid boundary conditions at the sliding surface to which signals were applied vertically in the form of SV-waves in order to produce horizontal shear within the landslide mass. The shear wave velocity was varied over the range of 100 m/s to 1000 m/s in steps of 50 m/s. Each mesh point is assumed to have 2 DOF in horizontal and vertical direction.

Results of the analyses of seismically induced slope deformation with the MRM can be discussed in qualitative and quantitative terms (Figure 2). Displacements calculated with MRM are maximum values of co-seismic displacements over the entire duration of the seismic input assuming visco-elastic behavior of soils. Concerning the qualitative aspect, internal and superficial displacement patterns appear to be identical for horizontal, vertical and resultant displacements; i.e. despite the application of different seismic scenarios and varying shear wave velocities, displacements concentrate around the main angular point of the landslide mass without any exception.

Quantitatively however, the intensities of displacements within these patterns reveal a strong dependency on the applied signal and shear wave velocity; i.e. the pattern gradient expands or shrinks according to the applied combination of signal and considered shear wave velocity. Lower shear wave velocities generally cause higher displacements due to a higher impedance contrast between the landslide mass and the underlying bedrock.

As for absolute values, the second column of Table 3 lists the greatest values of all horizontal displacements (dx) along the slope surface per signal. It can be seen that the values are greater of roughly two orders of magnitude compared to the results obtained with the Newmark-Method (1965) ranging from 1.0 to 65.3 cm.

Table 3. Greatest values of displacement for different methods and geometries along the slope surface.

	Newmark-Method (1965) (rigid block model)	Modal Recombination Method (simplified geometry)	Finite Difference Method (simplified geometry)	Finite Difference Method (fine geometry)
	downslope cumulative displacement	horizontal maximum displacement*	horizontal residual displacement*	horizontal residual displacement*
Signal	cm	cm	cm	cm
A	0.0	17.6	0.2	04.2
B	0.4	23.4	0.9	08.0
C	0.1	10.0	0.3	05.8
D	0.3	65.3	1.0	08.6
E	0.5	38.0	2.1	12.2
F	1.1	16.7	2.9	17.1
G	0.2	45.2	0.5	06.1
H	0.3	10.4	0.7	09.3
I	0.1	52.7	0.3	07.1
J	0.4	11.2	0.9	09.6
L	0.1	19.8	0.2	03.6
mean	0.3	28.2	0.9	08.3

* for vs = 300 m/s

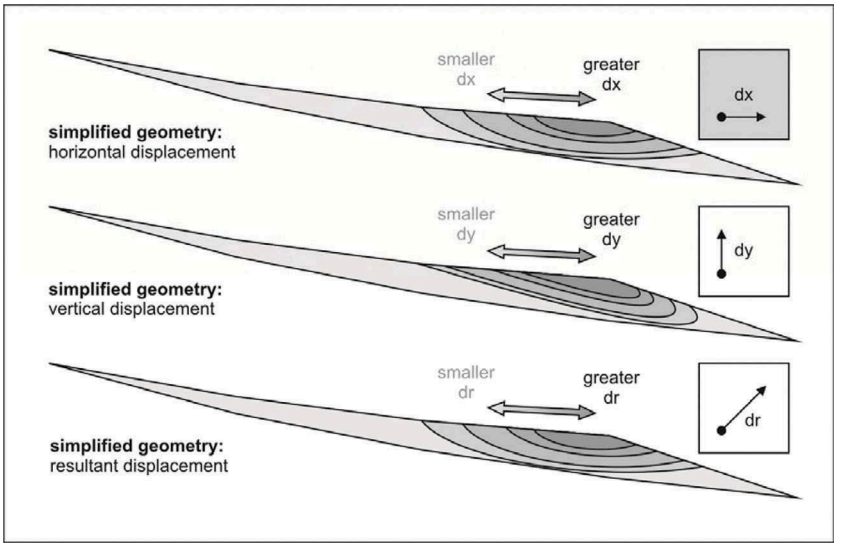

Figure 2. Schematic representation of maximum displacement patterns throughout the internal mesh grid obtained from the MRM. Dimensions of the cross sections are as in Figure 3a. The scheme distinguishes between horizontal (dx) and vertical (dy) displacements and the resultant displacement (dr). Displacement patterns only vary quantitatively – not qualitatively – with the applied signals and shear wave velocities, and hence there is no scale for the gradient.

3.3 *Finite Difference Method (FDM)*

Similar to the software CESAR-LCPC 2D, the software FLAC 2D also accounts for material properties (Table 1) such as shear wave velocity, Poisson's Ratio, shear modulus and bulk modulus. The model layout consists predominantly of a square grid for the simplified and the fine geometry with a spacing of 1.0 m, free field boundaries at the model sides and quiet boundaries at the model base to which signals were applied vertically in the form of SV-waves to produce horizontal shear within the landslide mass. For the landslide mass the only considered shear wave velocity was fixed to 300 m/s, whereas the shear wave velocity of the underlying bedrock was set to 1000 m/s (Table 1).

Again, results of the analyses of seismically induced slope deformation with the FDM can be discussed in qualitative and quantitative terms (Figures. 3a-b). Displacements calculated with the FDM are final permanent plastic displacements cumulated at the end of the entire duration of the seismic input. Already the static analysis, which evaluates the slope stability without the influence of external loads, has shown different results for both geometries. It appeared that for the simplified geometry the main concentration of shear strain covers the sliding surface beneath the hatched zone extending over the main angular point and the lower two thirds of the landslide mass (upper subplot of Figure 3a). For the fine geometry, in contrast, the concentration of shear strain is located along the sliding surface beneath the hatched zone referring only to the toe of the landslide mass (upper subplot of Figure 3b). This difference of static behaviors entails also different dynamic behaviors of both geometries.

Concerning the qualitative deformation, two aspects are obvious. First, internal displacement patterns as well as superficial displacement curves indeed reveal a strong dependency on the applied signal; i.e. the zones experiencing major deformation clearly differ for both geometries (hatched zones in upper subplots of Figures. 3a-b). Second – and in contrast to the results obtained with CESAR-LCPC 2D –, deformation patterns are not identical but depend on the applied signal, what is representatively illustrated by the superficial displacement curves of signals E an H (two curves in lower subplots of Figures. 3a-b).

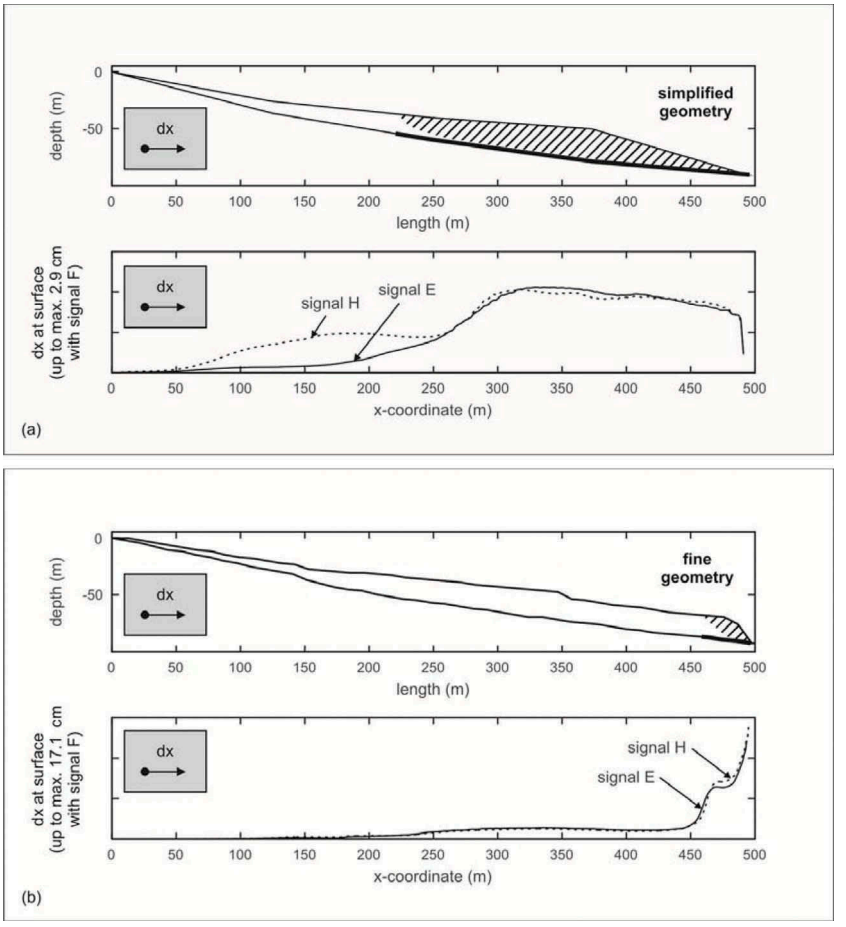

Figures 3a-b. Schematic representation of residual displacement patterns throughout the internal mesh grid (hatched zones in upper subplots) and along the slope surface (curves in lower subplots) obtained by the Finite Difference Method for the simplified (a) and the fine (b) geometry. The scheme only shows horizontal displacements (dx). Displacement patterns vary both quantitatively and qualitatively with the applied signals, and hence there is no scale for the ordinate of the lower subplots; exemplarily, only surface displacement curves of signals E (solid) and H (dashed) are shown. The thick lines beneath the hatched zones locate the major concentration of shear strain in the static phases of the analyses.

Qualitatively, intensities of displacement patterns are again dependent on the signal – however maintaining the imposed quantitative displacement pattern by the respective geometry.

Absolute displacement values are listed in the third and fourth columns of Table 3 as greatest values of all residual displacements (dx) along the slope surface per signal. Displacements obtained with the simplified geometry differ by roughly one order of magnitude from those obtained with the fine geometry; both range respectively from 0.2 - 2.9 cm and 3.6 - 17.1 cm. Positioned in these ranges, the results of the FDM fills the gap of two orders of magnitude between the Newmark-Method (1965) and the MRM.

4 CONCLUSIONS AND PERSPECTIVES

The evaluation of seismically induced slope deformation by means of the three methods has revealed significant differences with respect to signal- and shear-wave-velocity-dependency (where relevant) and concerning orders of magnitude of the obtained displacement values. It became obvious that only the FDM allows for clear signal-sensitive analysis of slope

deformation since internal deformation patterns show signal-dependent variations. Particularly, this latter aspect is important for precise engineering purposes and safety considerations; both the MRM and the Newmark-Method do not provide this essential level of detail.

Moreover, the comparative analysis of the three methods revealed a remarkable difference of displacement values regarding orders of magnitude. The Newmark-Method (1965) delivers the smallest results in the range of millimeters, what confirms the wide spread opinion that this method tends to underestimate seismically induced slope deformation (Rathje & Bray 2000, Rathje & Antonakos 2011, Lenti & Martino 2013, Gischig et al. 2015). Caution is thus suggested when making use of it. On the other extreme, the MRM yields surface displacements in the range of decimeters what seems by far too overrated. The most realistic results in the range of centimeters are obtained with the FDM. Although these results need to be confirmed by other case studies (work in progress), we believe they are general and not site specific.

However – within the FDM – the question of the representativeness of the cross section arises since displacement patterns differ considerably between the simplified and the fine geometry. Even though the displacement pattern obtained with the simplified geometry resembles the one obtained with the MRM, it should be kept in mind that a common assumption in numerical modeling states that finer models approximate reality better. If this is true for the case of the Diezma Landslide should be tested in a future analysis comparing a simplified and a fine geometry in 3D.

REFERENCES

Ambraseys, N.N. et al. 2004. Dissemination of European Strong-Motion Data. *Engineering and Physical Sciences Research Council of the United Kingdom* 2: CD-ROM collection.

Azañon, J.M. et al. 2010. Regional-scale high-plasticity clay-bearing formation as controlling factor on landslides in Southeast Spain. *Geomorphology* 120(1-2): 26–37.

Benito, M.B. et al. 2010. A new seismic hazard assessment in the region of Andalusia (Southern Spain). *Bulletin of Earthquake Engineering* 8(4): 739–766.

Delgado, J. et al. 2015. Unconventional pseudostatic stability analysis of the Diezma landslide (Granada, Spain) based on a high-resolution engineering-geological model. *Engineering Geology* 184: 81–95.

Domej, G. et al. 2017. Mean landslide geometries inferred from a global database of earthquake- and non-earthquake-triggered landslides. *Italian Journal of Engineering Geology and the Environment* 17(2): 87–107.

Gischig, V.S. et al. 2015. On the seismic response of deep-seated rock slope instabilities — Insights from numerical modeling. *Engineering Geology* 193: 1–18.

Google Earth 2015. Satellite image of the Diezma Landslide. Retrieved from Google Earth in December 2015.

ITASCA 2012. *Manual of FLAC 3D Version 5.0*. Minneapolis: ITASCA.

iTech & IFSTTAR 2014. *CESAR 2D Version 6.0 User's Manual*. Saint Maurice: iTech.

Jibson, R.W. et al. 2013. SLAMMER—Seismic LAndslide Movement Modeled using Earthquake Records. *United States Geological Survey Techniques and Methods* 12(B1): version 1.1 – November 2014.

Lenti, L. & Martino, S. 2013. A parametric numerical study of the interaction between seismic waves and landslides for the evaluation of the susceptibility to seismically induced displacements. *Bulletin of the Seismological Society of America* 103(1): 33–56.

Martínez-Solares, J.M. et al. 2013. *Actualización de mapas de peligrosidad sísmica de España 2012*. Madrid: Gobierno de España, Ministerio de Fomento.

Martino, S. et al. 2016. Application of a characteristic periods-based (CPB) approach to estimate earthquake-induced displacements of landslides through dynamic numerical modelling. *Geophysical Journal International* 206(1): 85–102.

Newmark, N.M. 1965. Effects of earthquakes on dams and embankments. Géotechnique 15(2): 139–160.

Pecker, A. 2018. *Dynamique des structures et des ouvrages*. Paris: École des Ponts - ParisTech.

Rathje, E.M. & Antonakos, G. 2011. A unified model for predicting earthquake-induced sliding displacements of rigid and flexible slopes. *Engineering Geology* 122(1-2): 51–60.

Rathje, E.M. & Bray, J.D. 2000. Nonlinear coupled seismic sliding analysis of earth structures. *Journal of Geotechnical and Geoenvironmental Engineering* 126(11): 1002–1014.

Rodríguez-Peces, M.J. et al. 2011. The Diezma landslide (A-92 motorway, Southern Spain): history and potential for future reactivation. *Bulletin of Engineering Geology and the Environment* 70(4): 681–689.

Varnes, D.J. 1978. Slope movement types and processes. In Schuster, R.L. & Krizek, R.J. (eds.). *Land-slides Analysis and control*. Washington D. C.: Transportation Research Board Special Report 176: 11–33.